1999-03

Acoustic-induced drag on a bubble

Chan, Eugene Joseph Pilpa

Monterey, California: Naval Postgraduate School

NAVAL POSTGRADUATE SCHOOL
Monterey, California

THESIS

ACOUSTIC–INDUCED DRAG ON A BUBBLE

by

Eugene Joseph Pilpa Chan

March 1999

Thesis Advisor: Andrés Larraza
Co-Advisor: Bruce C. Denardo

Approved for public release; distribution is unlimited.

REPORT DOCUMENTATION PAGE

Form Approved OMB No. 0704-0188

1. AGENCY USE ONLY *(Leave blank)*	2. REPORT DATE March 1999	3. REPORT TYPE AND DATES COVERED Master's Thesis

4. TITLE AND SUBTITLE

ACOUSTIC–INDUCED DRAG ON A BUBBLE

5. FUNDING NUMBERS

6. AUTHOR(S)

Chan, Eugene.

7. PERFORMING ORGANIZATION NAME(S) AND ADDRESS(ES)
Naval Postgraduate School
Monterey CA 93943-5000

8. PERFORMING ORGANIZATION REPORT NUMBER

9. SPONSORING/MONITORING AGENCY NAME(S) AND ADDRESS(ES)

10. SPONSORING/MONITORING AGENCY REPORT NUMBER

11. SUPPLEMENTARY NOTES The views expressed in this thesis are those of the author and do not reflect the official policy or position of the Department of Defense or the U.S. Government.

12a. DISTRIBUTION/AVAILABILITY STATEMENT
Approved for public release; distribution is unlimited.

12b. DISTRIBUTION CODE

13. ABSTRACT *(maximum 200 words)*

This work reports experiments that show that the drag on a bubble can be modified by the presence of isotropic, homogeneous broadband acoustic noise, when the band overlaps the bubble's resonance width. This constitutes an acoustic analog to the Einstein-Hopf drag on an electromagnetic dipole oscillator in the presence of isotropic and homogeneous electromagnetic fluctuations. In contrast with the electromagnetic Einstein-Hopf drag, band-limited acoustic noise can reduce the drag when the lower frequency of the spectrum coincides with the resonant frequency of the bubble. The modification of the drag experienced by a bubble in the presence of acoustic noise suggests possible applications to bubble migration and to heat transfer in a two-phase fluid. Depending on its size (i.e., resonant frequency), a bubble will experience less or more drag when the fluid is insonified with broadband noise, thereby modifying and possibly controlling bubble migration and heat transfer.

14. SUBJECT TERMS: Drag, bubble dynamics, analog to stochastic electrodynamics

15. NUMBER OF PAGES 40

16. PRICE CODE

17. SECURITY CLASSIFICATION OF REPORT	18. SECURITY CLASSIFICATION OF THIS PAGE	19. SECURITY CLASSIFICATION OF ABSTRACT	20. LIMITATION OF ABSTRACT
Unclassified	Unclassified	Unclassified	UL

NSN 7540-01-280-5500

Standard Form 298 (Rev. 2-89)
Prescribed by ANSI Std. 239-18 298-102

Approved for public release; distribution is unlimited.

ACOUSTIC–INDUCED DRAG ON A BUBBLE

Eugene Joseph Pilpa Chan
Lieutenant, United States Navy
B.S., University of California at Los Angeles, 1988

Submitted in partial fulfillment
of the requirements for the degree of

MASTER OF SCIENCE IN
APPLIED PHYSICS
from the

NAVAL POSTGRADUATE SCHOOL
March 1999

Author: [redacted]
Eugene Joseph Pilpa Chan

Approved by: [redacted]
Andrés Larraza, Thesis Advisor

[redacted]
Bruce C. Denardo, Co-Thesis Advisor

[redacted]
William B. Maier, Chairman
Department of Physics

ABSTRACT

This work reports experiments that show that the drag on a bubble can be modified by the presence of isotropic, homogeneous broadband acoustic noise, when the band overlaps the bubble's resonance width. This constitutes an acoustic analog to the Einstein-Hopf drag on an electromagnetic dipole oscillator in the presence of isotropic and homogeneous electromagnetic fluctuations. In contrast with the electromagnetic Einstein-Hopf drag, band-limited acoustic noise can reduce the drag when the lower frequency of the spectrum coincides with the resonant frequency of the bubble. The modification of the drag experienced by a bubble in the presence of acoustic noise suggests possible applications to bubble migration and to heat transfer in a two-phase fluid. Depending on its size (i.e., resonant frequency), a bubble will experience less or more drag when the fluid is insonified with broadband noise, thereby modifying and possibly controlling bubble migration and heat transfer.

TABLE OF CONTENTS

ACKNOWLEDGEMENTS

For since the creation of the world God's invisible qualities --- his eternal power and divine nature --- have been clearly seen, being understood from what has been made, so that men are without excuse.

Romans 1:20

This work is offered for the glory of God the Father of Jesus Christ, in whom alone we have eternal life.

I also wish to give recognition to:
My wife Amy for her love and prayerful support.
To Andrés Larraza and Donald Spiel, their enthusiasm and passion for physics are nothing short of contagious. From these men I learned the realities of research, its heartaches and its triumphs.
To Spencer French, my good friend and brother in Christ, his encouragement and support helped me economize my time in the lab. I could not have acquired the velocity data without him.
To Erich Chan, my own brother, by graciously offering his laptop for my use, saved me countless hours.
To members of the physics technical support team here at the Naval Postgraduate School:

Robert Sanders
David Grooms
George Jaksha
Donald Snyder

To these men, I am much indebted, their countless hours of support were instrumental in the creation the apparatus and success of this thesis.

Eugene Chan

I. INTRODUCTION

By 1910 it became very apparent that any attempt to apply classical arguments or the classical form of the equipartition theorem to the energy of mechanical or electromagnetic vibrations led directly to the Rayleigh-Jeans radiation law.

In an attempt to push further the contradiction between classical theory and experimental results, Einstein and Hopf (1910) considered a mass which contains an electromagnetic dipole oscillator in the presence of isotropic and homogeneous electromagnetic thermal fluctuations. Again, they proved that the assumption of energy equipartition for only the kinetic energy of a free particle led rigorously through classical theory to the Rayleigh-Jeans law.

Another important outcome of the Einstein–Hopf model was the realization that due to its interactions with the fluctuating electromagnetic field, a particle experiences two simultaneous and counteracting effects. In one, the particle experiences a random walk in phase space due to the electromagnetic thermal fluctuations, leading to an average *growth* in its kinetic energy. However, this accelerating effect is balanced by a dissipative, velocity dependent, drag force because of Doppler shifts. Einstein and Hopf appreciated the energy balancing action of the two opposing effects, which we understand today as a manifestation of the fluctuation–dissipation theorem (Callen and Welton, 1951).

Quantitatively , the model considers an oscillating dipole composed of a mass m and charge e, bound by an elastic restoring force to a mass M>>m of opposite charge. The equation of motion for a non-relativistic linear dipole is

described by the Abraham–Lorentz equation

$$\frac{d^2p}{dt^2} - \Gamma\frac{d^3p}{dt^3} + \omega_0^2 p = \frac{3}{2}\Gamma c^3 E_z \quad , \tag{1.1}$$

where p is the oscillator dipole moment, $\Gamma=2e^2/3mc^3$ is the radiation damping constant, c is the speed of light, and ω_0 is the characteristic frequency of the oscillator. In Eq. (1.1) we have assumed a dipole oriented along the z–direction, with E_z the z–component of the electric field of the random radiation.

In the derivation of the velocity–dependent Einstein–Hopf drag force, the spectrum of radiation loses its isotropy when viewed from a moving particle. Specifically, the fields experienced by the particle are Lorentz–transformed to a frame moving with the particle, and hence there arises a velocity–dependent force. If we assume translational motion along the x–axis, the force on the particle due to the interaction of the dipole is

$$F_x' = \frac{\partial E_x'}{\partial z'} p' - B_y' \frac{dp'}{dt'} \quad , \tag{1.2}$$

where primed quantities are to be evaluated in the particle's frame. Evaluating Eq. (1.2) for an electromagnetic thermal spectrum $\rho(\omega,T)$ leads to the velocity dependent drag force (Einstein and Hopf,1910; Boyer, 1969)

$$\mathbf{F} = -A\left[\rho(\omega_0, T) - \frac{1}{3}\omega_0 \frac{\partial \rho(\omega_0, T)}{\partial \omega_0}\right]\mathbf{v} \quad , \qquad (1.3)$$

where A is a positive constant, **v** is the velocity of the particle, and the spectrum is evaluated at the characteristic frequency of the oscillator. In thermodynamic equilibrium the expression in brackets is non–negative, and vanishes for the special case of a spectrum proportional to the cube of the frequency. This corresponds to the zero–temperature limit value of $\rho(\omega,T=0)$, which is referred to as the zero–point field (ZPF) spectrum, and which has the form

$$\rho(\omega) = \rho(\omega, T = 0) = \frac{\hbar\omega^3}{2\pi^2 c^3} \quad , \qquad (1.4)$$

where $\hbar$ is the reduced Planck's constant.

The ZPF spectrum is a homogeneous, isotropic, Lorentz–invariant spectrum. Consequently, a polarizable particle cannot suffer velocity–dependent forces due to its motion through the ZPF. Thus, for a ZPF spectrum (1.4) the drag force (1.3) vanishes and the particle's translational kinetic energy would increase unchecked because the accelerating effect due to the fluctuating field is not balanced by a dissipative force. This has been proposed as an acceleration mechanism for cosmic rays (Rueda, 1978). The possibility of the ZPF as a stochastic acceleration mechanism for cosmic rays is appealing because the power law relating the number density with the energy of cosmic rays suggests a

common acceleration mechanism for all particles, or at least those in the ranges where the exponent of the power law remains constant.

The notion that acoustic noise can test, by analogy, predictions due to stochastic electrodynamics and to ZPF effects has been established recently by measurements of the force law between two rigid, parallel plates due to the radiation pressure of broadband acoustic noise (Larraza *et al*, 1998; Larraza and Denardo, 1998). This measurement constitutes an acoustic analog to the Casimir effect (Casimir, 1948) which is the force of attraction between two closely spaced uncharged parallel conducting plates due to the ZPF. In both the ZPF Casimir effect and the acoustic analog, the force between the two plates can be understood in terms of the radiation pressure exerted by the field. However, in contrast to the ZPF Casimir effect, band limited acoustic noise can cause the force to be attractive *or* repulsive as a function of separation between the plates.

In this work, we report on experiments that show that the drag on a bubble can be modified by the presence of isotropic, homogeneous broadband acoustic noise, when the band overlaps the bubble's resonance width. This constitutes an acoustic analog to the Einstein–Hopf drag. To our knowledge, our observations are the first of this effect. A preliminary theoretical analysis (Larraza, 1999) has shown that small–amplitude oscillations of a bubble in an acoustic field are described by an equation of motion that is analogous to the Abraham–Lorentz equation for an oscillating dipole:

$$\frac{d^2V}{dt^2} + R\frac{dV}{dt} + \omega_0^2(V - V_0) = \frac{S_0^2}{m_e}[P_0 - P(t)] \quad , \qquad (1.5)$$

where V is the oscillating volume of the bubble, V_0 its equilibrium volume, R is a measure of the damping effects (thermal, radiation, and viscous), ω_0 is the characteristic frequency of oscillations of the bubble, S_0 is the equilibrium surface area of the bubble, m_e is the entrained mass of the fluid, P_0 is the hydrostatic ambient pressure, and P(t) is the acoustic pressure of the random noise field at the surface of the bubble. Equation (1.5) is applies for wavelengths of sound much larger than the bubble radius.

Similarly, the translational motion of the bubble in the acoustic field is determined by the force

$$\mathbf{F}' = V'\nabla P' \qquad (1.6)$$

where the fields experienced by the bubble are Galilean–transformed to a frame moving with the bubble, yielding a drag similar to Einstein–Hopf's.

As in the case of the acoustic analog to the Casimir effect, band-limited acoustic noise can cause effects not considered in the electromagnetic Einstein-Hopf drag. Our preliminary observations show that, for some spectral shapes in which the lower frequency of the spectrum coincides with the resonant frequency of the bubble, there is surprisingly an increase in the terminal velocity of a bubble. That is, the noise exerts a *negative* drag on the bubble in this case.

Besides providing the acoustic analogs to the Einstein–Hopf drag, our investigations can thus lead to analogs to mechanisms for stochastic acceleration of charged particles that are used to explain cosmic rays.

In Chapter II of this thesis we describe the apparatus and experimental techniques used to measure the acoustic–induced drag on a bubble. In Chapter III we present preliminary results of the effects of drag on a bubble due to broadband noise, and suggest future work.

II. APPARATUS

In this chapter we describe the apparatus, instrumentation, and experimental techniques used to measure the dynamics of a buoyant bubble in the presence of broad–band noise. As shown in Figure 2.1, the main components of the apparatus are two broad-band sources of sound and a pipette which, connected to a pressurized nitrogen gas tank, injects a controllable stream of nitrogen bubbles.

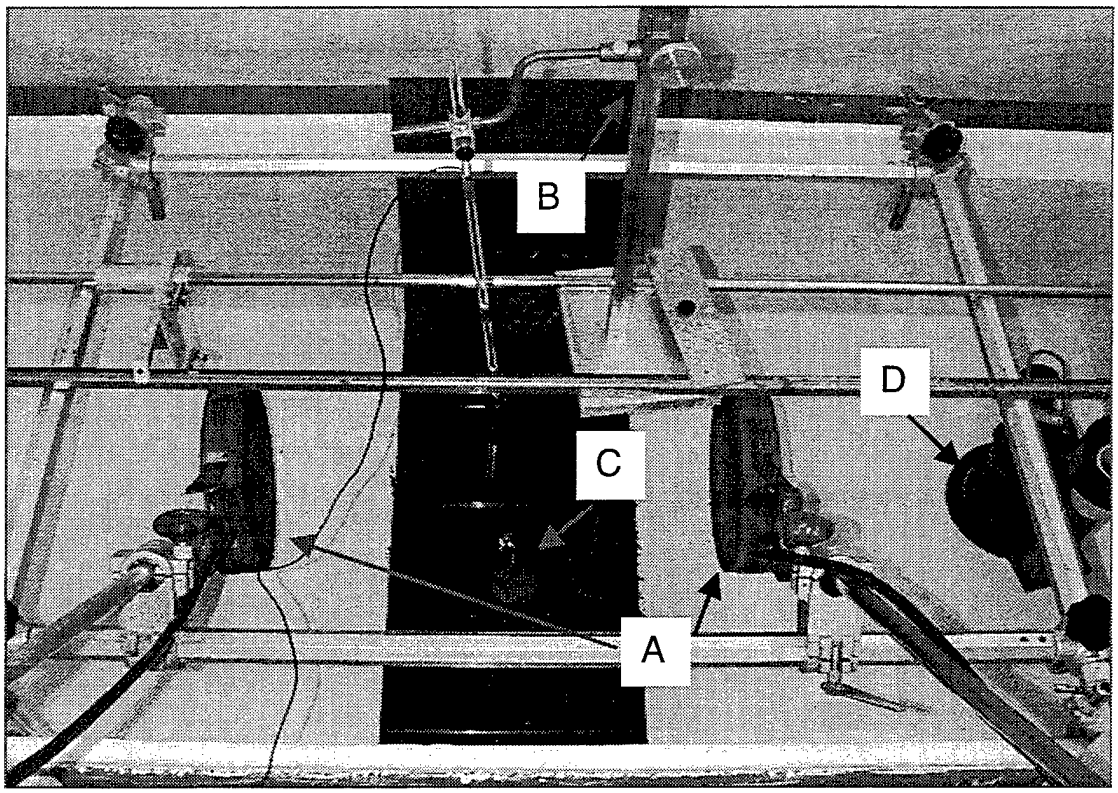

Figure 2.1. Overhead view of the basic tank configuration. The tank is made of wood reinforced fiberglass, with inner dimensions 1.78 x 0.86 and 0.61 m in depth. The water depth is kept at 0.51 m. (A) The left and right source transducers are visible. (B) The hydrophone and vertical positioner are in the center view. (C) A pipette holder is set on a lab–jack that rests on the floor between the source transducers. (D) At the far right is a submerged water filtration system and pump.

A. THE ACOUSTIC ENVIRONMENT OF THE BUBBLE

The acoustic environment is created within a tank constructed of wood reinforced fiberglass. The inner dimensions of the tank are 1.78 x 0.86 m and 0.61 m in depth. The water depth is kept at 0.51 m, conveniently chosen to coincide with the upper rim of the tank-viewing window. This window facilitates viewing and photography of the bubbles. The window is a 6 mm thick glass 0.37 $\times$ 0.27 m and was fashioned from the center of one side of the tank. Hospital bed supports were placed on the lip of the tank to support transducers and sensing probes. Each source transducer was secured by the use of locking clamps. This made it easy to position them along the length, width, and depth of the tank. The sensors were also adjustable along the tank length and width with additional fine adjustment in depth.

Particulate matter within the water makes the pipettes susceptible to clogging. Furthermore, scattering of light off these particles interferes with data gathering. To lessen these effects a submergible water purification system was placed within the tank. It consists of a recycling pump and filters. A plastic hood was used to cover the exterior of the tank to minimize dust particles entering the water.

The three primary considerations for the measurements that we report in this work are the spectral shape of the acoustic noise field, the degree of homogeneity of the noise field, and the bubble size. As stated in the Introduction, the spectral range of the spectrum determines the acoustic–induced drag on a bubble. The homogeneity of the acoustic field along the bubble ascent

path is mainly dictated by transducer placement and frequency range. Ensuring acoustic homogeneity along the ascent path of the bubble negates the possibility of bubble accelerations caused by gradients in the average sound intensity.

From the dimensions of the tank, the geometry of the source transducers, as well as their output limits, we determined that a the noise field in a vertical column of water along the bubble's path was homogenous in the frequency band from 3 to 24 kHz. Thus for a given spectral band of frequencies of the noise that would yield a homogeneous spectrum over a range of distances, the bubbles were confined to certain sizes. These sizes were constrained also by the need to minimize hydrodynamic instabilities which cause unwanted horizontal perturbations of the bubble during its ascent. Limiting the diameter the bubble below 1.0 mm minimizes the hydrodynamic instabilities. On the other hand, exit rates for bubbles of sizes much less than 0.5 mm become difficult to control and so such bubbles were avoided. These considerations limited the study to bubble sizes of the order of 0.5 ~ 1.0 mm-diameter. For these sizes, the bubble resonant frequency is in the range of 6 to 13 kHz (Apfel, 1996).

1. Transducers and Drivers

Two Navy Model F-33 piezoelectric transducers produce the acoustic noise within the tank. Each transducer is driven separately by a General Radio Company Model1390-B random noise generator. The generator outputs are passed through a 115 dB/octave bandpass filter (SR650) set to the desired band within the 3 octaves from 3 to 24 kHz. Each filtered output is amplified by a power amplifier (Instruments Inc. Model L2). The signal input to and output from

this amplifier were monitored via a HP 34401A multimeter. Maximum amplitude is limited by impedance matching between amplifier and transducer. Amplifier outputs are kept at 80 VAC to avoid overloading the amplifier. A schematic of the instrumentation is outlined in Figure 2.2.

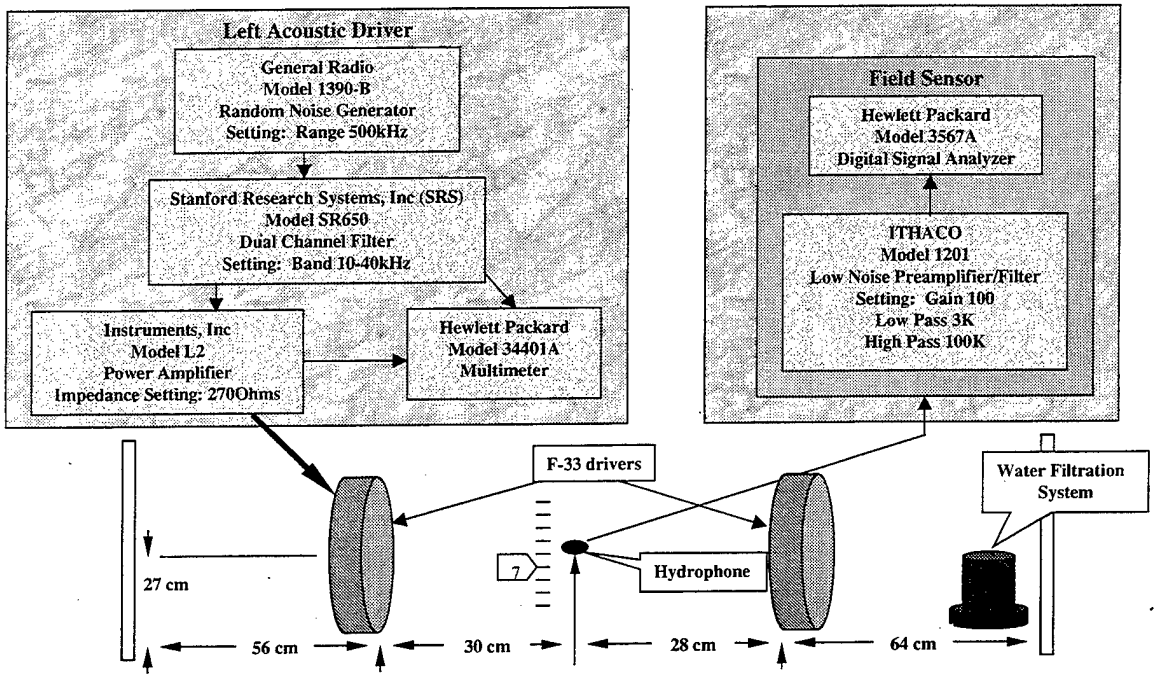

Figure 2.2. Instrumentation and transducer locations. The bubble's ascent path is along the markings that determine the locations where the acoustic noise was measured.

2. The Acoustic Field

Mapping the horizontal and vertical acoustic field within the tank was accomplished using an EDO Model 6600 omnidirectional hydrophone. Spherical in shape, the hydrophone was placed at the end of a plastic rod. Fine adjustments in depth are accomplished by using a sliding bar, which is positioned on two support beams above the water. When mapping, the hydrophone was

constrained to move vertically in depth along a line intersecting the axis of symmetry between the two transducers.

The drivers are positioned asymmetrically along the lengthwise center axis of the tank. This configuration discourages some modes of the tank. First placed symmetrically about the geometric center of the tank, the drivers were gradually offset from symmetry until the average variance in acoustic intensity at the hydrophone, along a wide frequency band (3 ~ 24 kHz) varied no more than 5 dB.

Once the horizontal position in the tank is selected, the sound field of the ascent path can be mapped. Acoustic field averages were measured at 16 vertical positions, spaced 1 cm apart, along the potential ascent path. The lowest position is labeled as position 0, and position 8 corresponds to the height along the common axis of the two drivers. The average acoustic field intensity at each position was determined from 100 samples. The noise spectra reveal the location and length along the ascent path providing the most uniform acoustic field. In this study, the bubble resonance frequencies were typically of the order of 10 kHz. In this configuration, conditions are nearly homogenous along positions 4 through 12. Figure 2.3 is a plot of the acoustic field intensity at these locations. Once the general field characteristics are determined, bandwidth and amplitude are then adjusted to accommodate the resonant frequency of the particular bubbles.

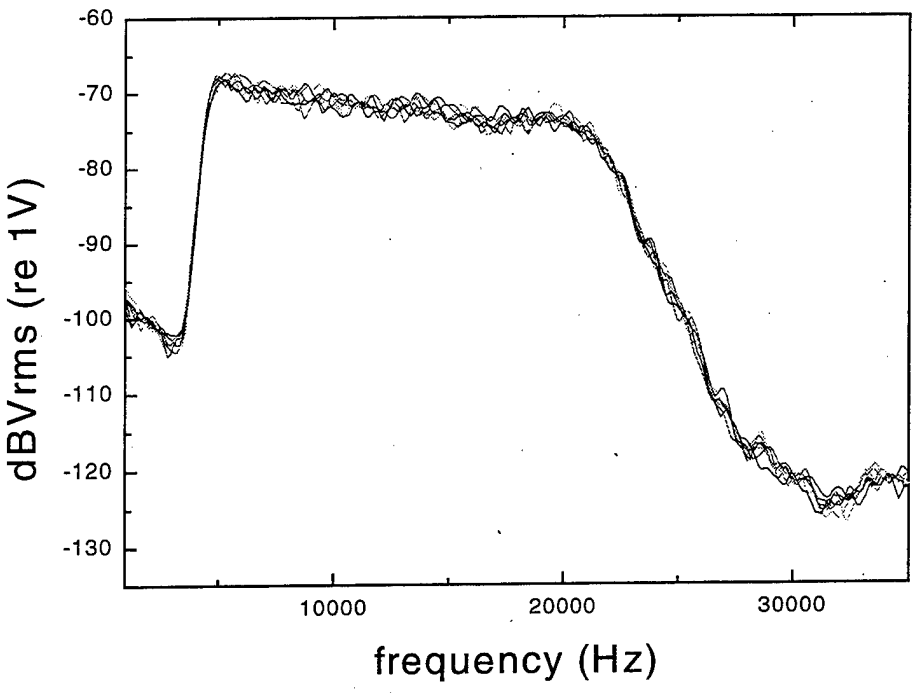

Figure 2.3. Acoustic field intensity measurements at vertical locations 4 through 12. The spectrum is nearly flat in a band of frequencies between 3 to 24 kHz. Well represented by the figure is the fact that the noise intensity is essentially homogeneous along this column of water.

B. GENERATION AND CONTROL OF BUBBLES

Ensuring the ability to produce bubbles of consistent resonant frequency and exit rates was a challenge that required several stages of evolution. This was due primarily to preferences, explained earlier, which required bubble sizes much smaller than had earlier been attempted with known techniques. In general, the smaller the bubble the smaller the inner diameter of the pipette.

1. Pipette Construction

A satisfactory method adapted from Blanchard and Syzdek (1977), uses glass pipettes fashioned by heating glass tubing with a bunsen burner and drawing out by hand. Our tubing had a 5.0 mm outside diameter and an inside diameter of 0.3 mm. After heating and drawing out by hand, the end result was a pipette tip resembling an optical fiber. Under the scrutiny of a microscope, the inner diameter of the pipettes are typically found to be 0.5 to 3.0 μm, which are capable of producing bubbles of the order of 100 μm-diameter. These were detectable only when released rapidly in large quantities and resembled clouds of smoke. This, of course, is a far smaller bubble than necessary for this investigation. Since the inner diameters of the pipettes increase with distance from the tip, larger apertures are attainable by cutting off the end of the pipette, an increment at a time, until the required aperture is obtained. The use of commercial pipette pullers can minimize variations in aperture diameter and neck length. There is now such equipment at the Naval Postgraduate School which is programmable and capable of heating glass pipettes and stretching them to desired length and width. Though not available in the course of this study, such equipment may prove a useful utility in future work.

A pipette holder (Figure 2.4) is used to position the pipette within the tank and to connect it to a pressurized gas (nitrogen) tank. Forcing the gas through the pipette aperture produces bubbles. The gas pressure required for each pipette varied, but was typically 15 psi or less.

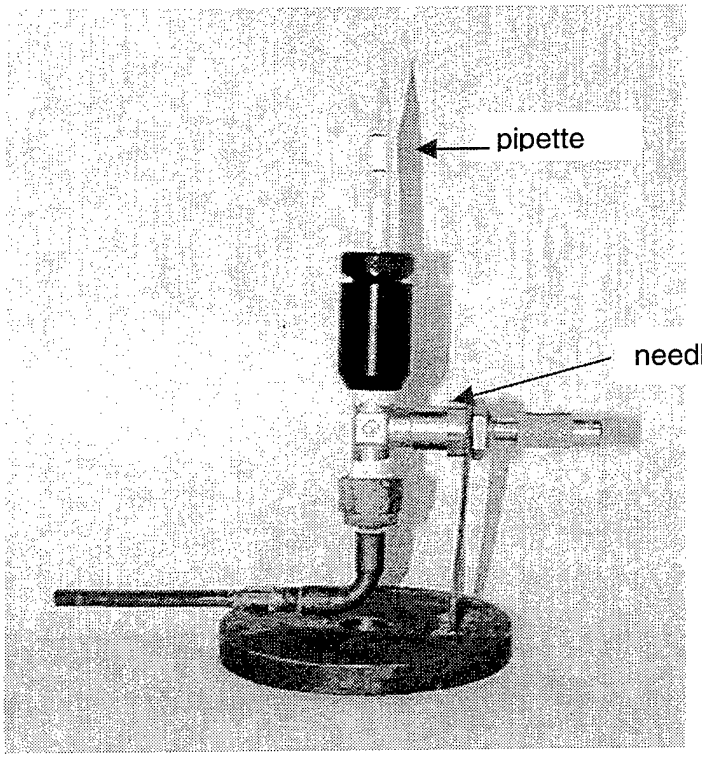

Figure 2.4 . Pipette and pipette holder. The needle valve was constructed into the holder with the hope of additional rate control. However, the needle valve quickly became corroded and was of little use. It was kept in the full open position throughout the experiment.

2. Reliable and Consistent Bubbles

Control of individual bubble exit rate was important to facilitate photographic data acquisition. Gas pressure was controlled with a Fairchild Industrial Company Model 10 Pressure Regulator. Gas pressure regulation controls bubble exit rate. A fine needle valve was installed inline after the pressure regulator with the expectation of individual control on bubble exit time. Currently the best control achieved is a bubble exit rate of approximately 2 bubbles per second for bubble sizes whose resonant frequencies are in the range of 8 to 15 kHz.

Ensuring the long lifetime of a pipette was critical in obtaining reproducible data. Each pipette created bubbles of a given resonant frequency. Maintaining the same pipette throughout data acquisition was hampered because of the extremely small apertures (≈6 μm) needed to create bubbles with the desired resonant frequency. With the use of an inline air filter and water purification system, the problem of pipette clogging was reduced slightly. With pipette aperture sizes as small as 6 μm, the normal useful life of a pipette was approximately 12 hours if not a couple of hours. Typically, for a successful acquisition run, once a pipette is inserted into the water 2 to 4 hours are required to stabilize the bubble rate and determine resonant frequency and another 4 to 6 hours to obtain ascent data.

Although each bubble producing technique provided reproducibility within a defined acoustic environment, none was capable of maintaining constant bubble sizes when the field strength was varied. However this variance in bubble size was observed to occur only when the acoustic band generated in the tank included frequencies above the line-width of the bubble.

C. BUBBLE DETECTION SYSTEM

Bubbles separating from the pipette undergo a characteristic oscillation (Longuet–Higgins, et al. 1991), which in an environment free of acoustic perturbations defines the bubble resonant frequency and its quality factor. Because the EDO hydrophone was not sensitive enough to measure the acoustic output from the oscillating bubble, we build a capacitance hydrophone. The

hydrophone (Figure 2.5) consists of a cylindrical Lucite block (b) machined to house a copper plug (a) in one side. The face of the copper plug is flush with the Lucite and was bead blasted to give the copper a rough surface. Atop this face is laid a thin sheet of mylar. The mylar is glued at its edges to the surrounding Lucite case. The outermost surface of the mylar is pre-coated with a thin film of aluminum and its edges silver painted to help prevent leaks and to facilitate connection to a ground wire (c). Essentially these components form a capacitor with the mylar acting as a dielectric between two conducting surfaces, the outer aluminum surface of the mylar and the surface of the copper plug. The aluminized mylar surface and copper plug are kept at a constant charge corresponding to 300V. Pressure variations caused by a bubble exiting the pipette disturb the mylar surface and are sensed as a varying capacitance.

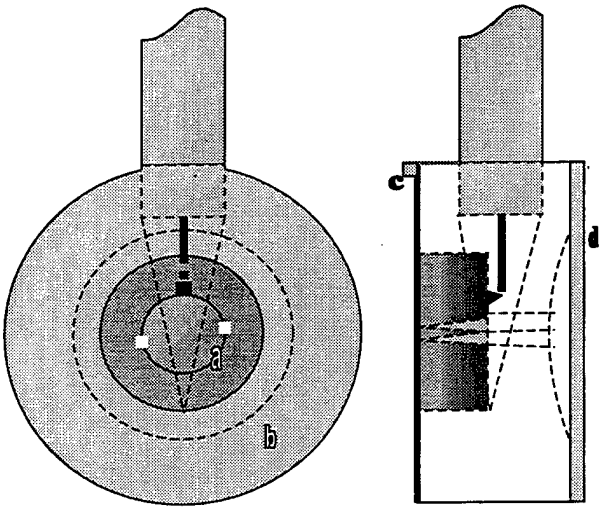

Figure 2.5. Hydrophone developed for this study. A photodiode was attached in order to trigger data samples when the bubble was exposed to the acoustic field.

A shallow concentric circle was etched into the copper surface of the plug along with two small holes connecting the front (bead blasted) surface of the copper plug with the back of the Lucite casing. The backside of the Lucite casing is slightly concave and is covered with a latex diaphragm (d). This was done to compensate for pressure differences at depth and prevented flooding through the mylar side of the hydrophone, which, experience showed, was necessary. For added protection, as the aluminized mylar was easily subject to tears and corrosion, the surface of the aluminum was painted with clear furniture varnish.

Constructed as part of a circuit using a transimpedance amplifier, a diode connected to the hydrophone senses the incoming light from a diode laser, positioned externally. The laser beam is directed through the tank-viewing window and aimed directly at the tip of the pipette in line with the photo diode. A bubble exiting the pipette will cross the beam and cause a fluctuation in light at the diode, thus initiating a trigger. Initial alignment and triggers are accomplished in the sound free environment where the trigger signal is adjusted to synchronize with the bubble signature as it pinches off the pipette. The triggered output of the hydrophone is then recorded by a 1.5 GHz oscilloscope (HP *infinium*) from which the bubble's resonant frequency and quality factor can be determined. A schematics of the bubble acoustic sensor is shown in Figure 2.6.

BUBBLE ACOUSTIC SENSOR CONFIGURATION

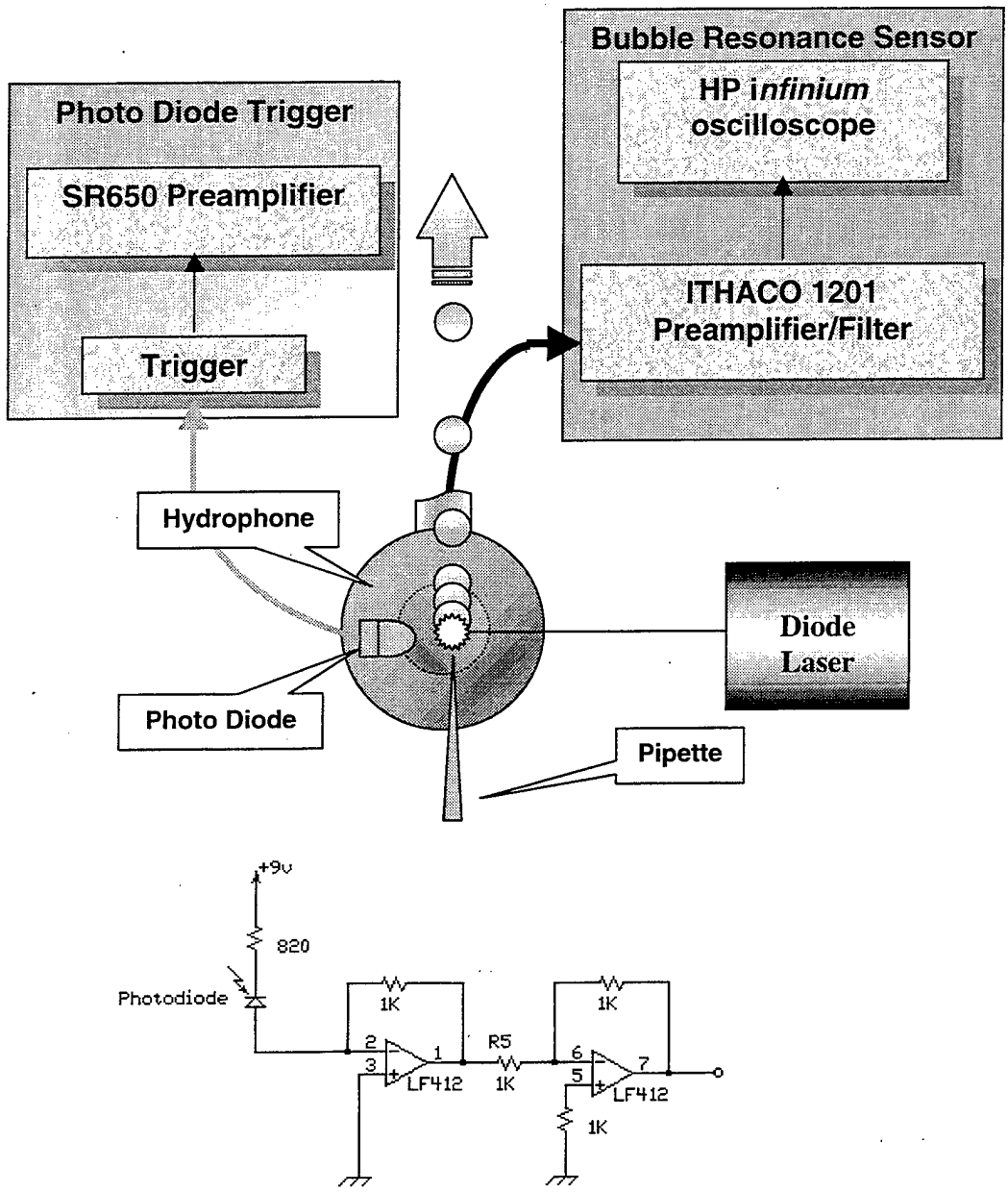

Figure 2.6. Instrument configuration for the hydrophone and photo diode. The transimpedance circuit is shown at the bottom of the figure.

D. PHOTOGRAPHIC DATA ACQUISITION

The use of photography lends well to the service of capturing velocity and acceleration information. In our case this was accomplished with the use of a digital camera (Kodak DC120) and two synchronized stroboscope light sources.

Setting a higher strobe frequency relative to the bubble exit rate, the camera shutter speed can be adjusted to allow successive images of the same bubble onto a single photograph. The distance between successive bubble images can be measured directly off the photograph. Since the inverse of frequency gives the time between successive strobe flashes, both distance and time information is available. It is then a simple calculation to determine velocity and acceleration data from one photograph.

Problems regarding exit rate control persisted throughout the experiment. Nevertheless, obtaining exit rates of approximately 2 s^{-1} to 10 s^{-1} are possible and can be easily coordinated with strobe and camera. Exit rate control is accomplished by adjustment of the gas pressure. Pressure requirements are unique to the each pipette, but are typically between 1 and 15 psi. There exists a relationship between the necessary pressure required to release a bubble and aperture size (Blanchard and Syzdek, 1977). However, in this study, the pressure required was vastly different between pipettes of the same aperture. The only characteristics noted different in each case is the thickness of the pipette at the aperture, the relative length of the stretched portion, neck, of pipette and possibly pipette cleanliness. The first two differences are probably due to method of construction, specifically; the speed at which the pipette was

pulled and lengthened after heating and /or the location along the lengthened pipette chosen to be the tip.

Once the exit rate of the bubbles is stabilized for a particular pipette the strobe frequency is set to obtain sufficient images to determine the ascent velocity and acceleration. Preferences for strobe frequency ranged from 150 to 300 kHz for bubbles of ascent velocities roughly 5 to 10 cm/s.

Strobe position too was a crucial factor in obtaining clear photographic data. Scattering of light was a concern. Forward scattering provided the best images. In order to optimize the images, a strobe was placed aft of the ascent path above the water. The strobe was aimed to provide the maximum backlight as possible without shining directly into the camera. The tip of the pipette was adjusted to optimize lighting given the constraint that the pipette position was within the preferred length of the ascent path.

The obvious advantages of digital cameras are that fine adjustments in lighting, focus, strobe rate and shutter speed can be made with relative ease. Photographs are quickly accessible on computer where they can be analyzed and digitally manipulated. The DC120 was an excellent camera for photographic data acquisition. However, pixel density of this camera may render images with insufficient resolution. In the future a film camera may have to be used in order to obtain better resolution.

III. RESULTS AND CONCLUSIONS

A buoyant bubble in the presence of broad–band acoustic noise can exhibit an enhancement in its inertia and an added drag due to the interactions with the noise. With the field band centered about the resonance line of the ascending bubble, the ascent velocity of a 10.7 kHz bubble was examined in three differing environments here designated as cases *'a', 'b',* and *'c'*. Case *'a'* corresponds to an acoustic noise–free environment. In this case, the terminal velocity was measured to be 8.3 cm/s. Cases *'b'* and *'c'* correspond to an acoustic noise with an rms pressure 714 Pa in a band of frequencies between 8 to 10 kHz, and 9 to 11 kHz respectively. Thus only in case *'c'* the acoustic noise was in a band of frequencies which incorporated the frequencies of the bubble line width. In case *'b'* the bubble's terminal velocity was measured to be equal to the case of noise–free environment, or 8.3 cm/s. In case *'c'* the terminal velocity was 6.5 cm/s, a decrease of 22 percent.

The decrease in terminal velocity is not due to a different size bubble that may occur as a result of the noise affecting bubble generation. We ruled this effect out by generating a bubble in the presence of noise and then immediately switching the noise off. We then observed that the terminal velocity was the same as in the case when there is never any noise.

Because of the inherent difficulties, described earlier, only one pipette functioned long enough to capture each of the three cases above on film. The following discussion is based on this data.

A. BUBBLE RESONANT FREQUENCY AND QUALITY FACTOR

The acoustic signal of bubbles pinching off the end of this particular pipette was recorded (Figure 3.1), and the bubble's resonant frequency was determined to be 10.7 kHz. The quality factor *Q* was determined first by measuring the amplitudes of the signal crests and their location in time. The natural logs of these amplitudes were then plotted against time and fitted linearly (Figure 3.2). The time constant τ is defined as the inverse of the slope of this fit, where it takes τ seconds for the bubble signal to decay to *1/e* of its maximum amplitude. For this particular pipette, the bubble's time constant τ was 2.19×10^{-4} sec. Thus the Q of the bubble is $Q = \pi f \tau = 7.4$ corresponding the line width $\Delta f = f/Q = 1.5$ kHz. In this case, the ideal band of frequencies of the noise for this bubble is between 9.95 to 11.45 kHz. The actual band used for case *'c'* was 9 to 11 kHz.

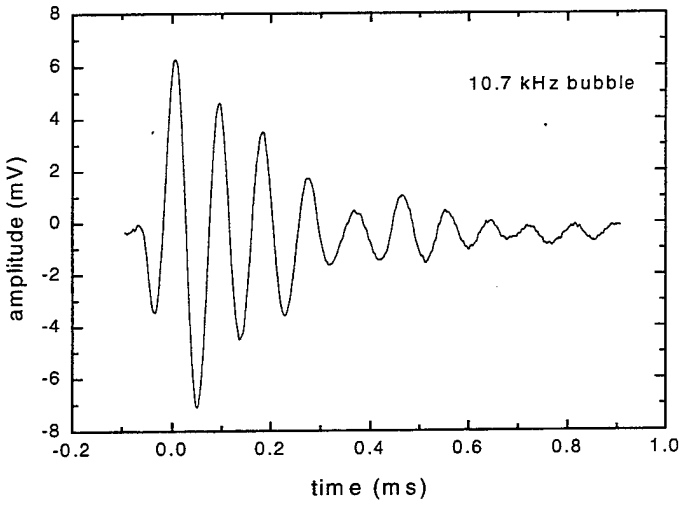

Figure 3.1. Plot of the acoustic signal for a 10.7 kHz bubble.

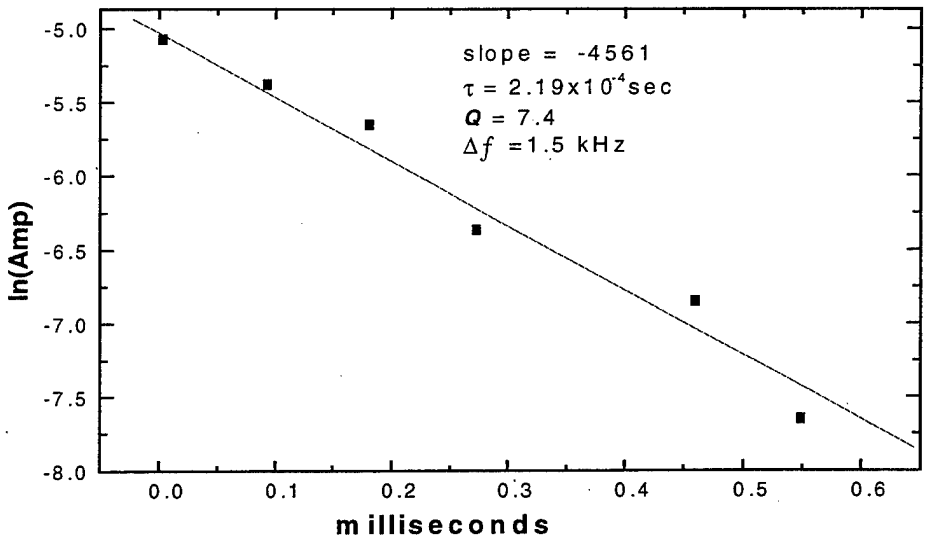

Figure 3.2. The Q of the bubble is determined first by reading off Figure 3.1 the amplitudes of the signal crests and their location in time. The natural logs of these amplitudes is then plotted versus time. A linear fit yields the bubble's decay time τ from which the value of $Q=\pi f\tau$ can be calculated.

B. VELOCITY FROM PHOTOGRAPHIC DATA

The bubble ascent photographs in Figure 3.3 were obtained with a digital camera using stroboscopic techniques (Chapter II). The photographic record for cases *'a'* and *'b'* shows the stroboscopic images of eight moving bubbles, while case *'c'* corresponds to the stroboscopic image of two moving bubbles. For each case the shutter speed was adjusted to bubble exit rate, to distinguish between individual bubbles, and the strobe frequency maintained at 150 Hz.

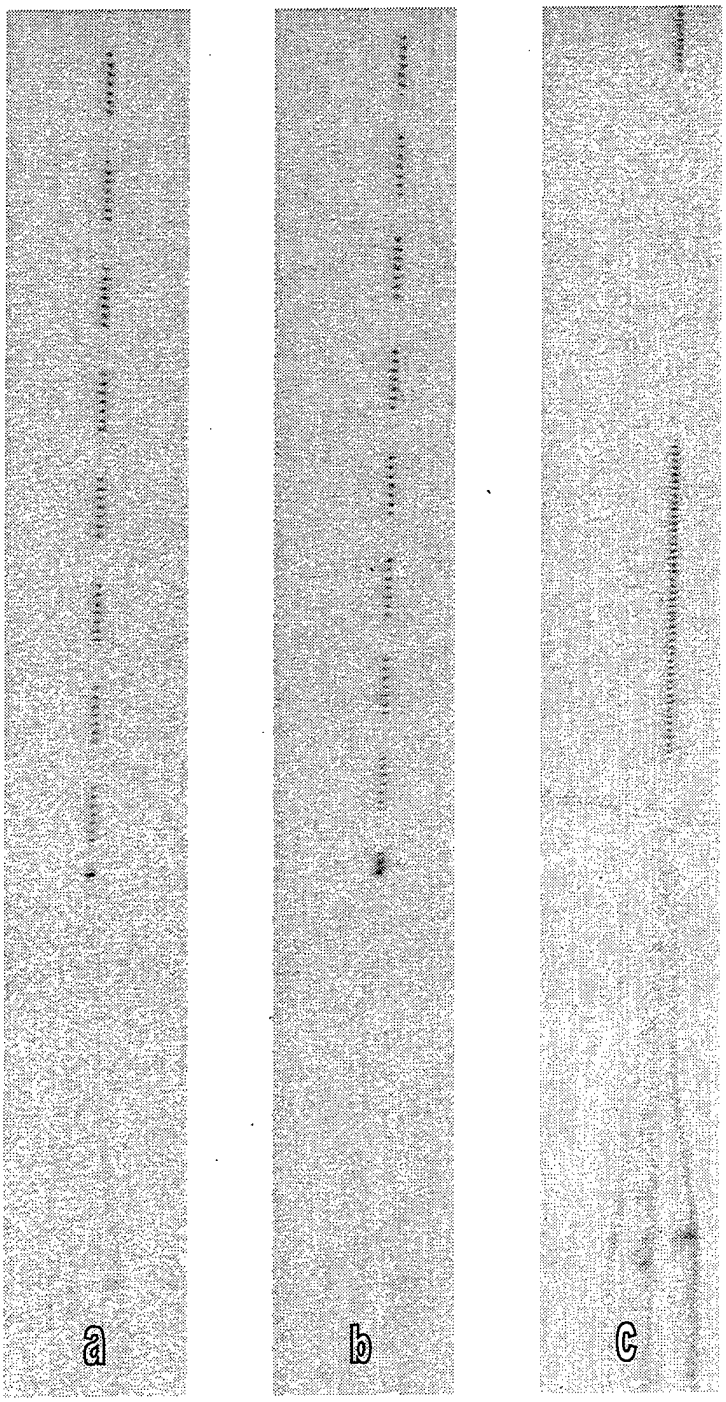

Figure 3.3. Stroboscopic photographs of ascending 10.7 kHz bubbles: a) Each bubble moves in the absence of acoustic noise, b) the acoustic noise is in a band of frequencies between 8-10 kHz, and c) the acoustic noise in a band of frequencies between 9-11 kHz. The strobe light is set at 150 Hz. Note the marked reduction in velocity in 'c' compared to cases 'a' and 'b'. Shown in the photograph is the profile of the pipette.

The distance between bubble exposures was determined by measuring the light intensity for each pixel along the line of ascent. For each case, the maximum pixel intensity is determined with respect to its distance from the pipette aperture. Distances are calibrated from a picture of a millimeter–graded ruler placed on the path of the ascending bubble. The time between each bubble image is the inverse of the strobe rate. 'Distance from the pipette' versus 'time' is plotted in the Figure 3.4. The ascent velocity is determined from the slope of the linear fit to the data.

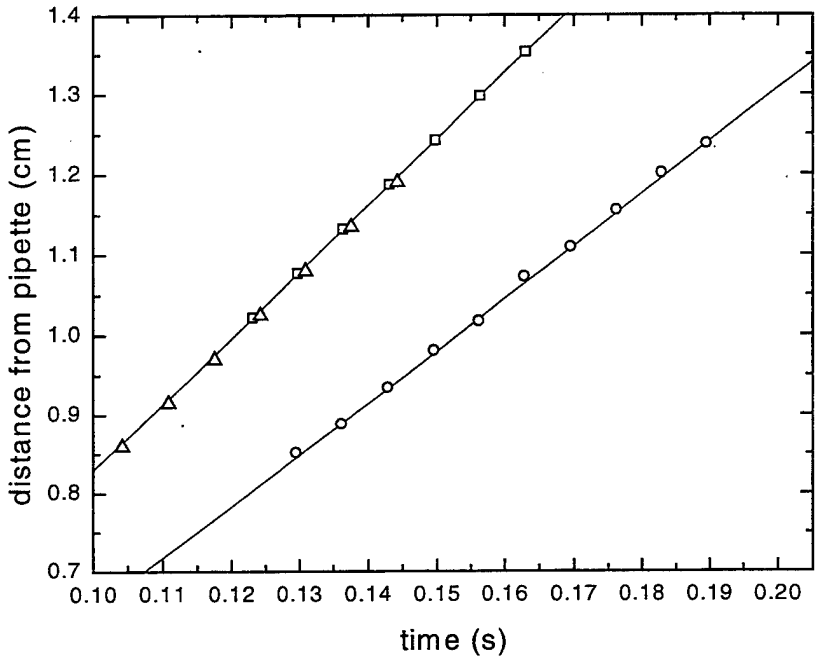

Figure 3.4. The data from figure 3.3 represents a sampling of images 0.85 to 1.40 cm above the pipette aperture. The slope of the fitted line indicates terminal velocities for: a) Δ no–noise corresponding to a terminal velocity of 8.3 cm/sec, b) □ noise in a band of frequencies between 8-10 kHz corresponding to a terminal velocity of 8.3cm/sec, and c) O noise in a band of frequencies between 9-11 kHz corresponding to a terminal velocity of 6.5 cm/sec. The rms pressure for both (b) and (c) corresponds to 714 Pa.

C. CONCLUSIONS AND FUTURE RESEARCH

The difference in terminal velocities, evident between the case *'a'* and *'c'* photographs, shows that the drag on a bubble can be modified by the presence of isotropic, homogeneous broadband acoustic noise. Case *'b'*, on the other hand, established the observation that when the band of noise does not overlap the bubble's resonance width, the acoustic induced drag is absent. This is consistent with a preliminary theoretical analysis (Larraza, 1999).

However, the bubble in all cases accelerates to its terminal velocity. In addition to the Casimir effect, the properties of the ZPF have been explored to derive Newton's second law, and hence the origin of inertia (Rueda and Haisch, 1998). By monitoring the acceleration of a bubble in the presence and absence of the noise, we can determine if there exists an acoustic-induced inertia.

With some adjustments, the current photographic techniques may be sufficient to acquire acceleration data. Initial attempts photographing ascending bubbles using a Horseman camera are promising as they produced Polaroid photographs superior in quality and clarity to the digital images of this study. Visually, bubbles with resonant frequencies in the range 8 to 11 kHz, appear to accelerate within the first 3 centimeters of ascent. Magnification of this area is recommended and can be accomplished with a Nikon N6006 35mm camera and zoom lens, which is now available.

LIST OF REFERENCES

Apfel, R. "Sonic effervescence: A tutorial on acoustic cavitation," *J. Acoust. Soc. Am.* **101**, 1227-1237, 1994.

Blanchard, D.C., and L. D. Syzdek, "Production of air bubbles of a specific size" *Chem. Eng. Sci.* **32**, 1109-1112, 1977.

Boyer, T., "Derivation of the Blackbody Radiation without Quantum Assumptions," *Phys. Rev.* **182**, 1374-1383, 1969.

Callen, H. B., and T. A. Welton, "Irreversibility and Generalized Noise" *Phys. Rev.* **83**, 34-40 1951.

Casimir, H. B. G., "On the Attraction Between Two Perfectly Conducting Plates," *Proc. Kon. Ned. Akad. Wetensch.* **51**, 793-796, 1948.

Einstein, A. and L. Hopf. "Statistische Untersuchung der Bewegung eines Resonators in einem Strahlungsfeld" *Ann. Physik* (Leipzig) **33**, 1105-1115, 1910.

Larraza, A, C. D. Holmes, R. T. Susbilla, and B. Denardo, "The force between two parallel rigid plates due to the radiation pressure of broadband noise: An acoustic Casimir effect," J. Acoust. Soc. Am. **103**, 2267–2272, 1998.

Larraza, A. and B. Denardo, "An acoustic Casimir effect," Phys. Lett. A **248**, 151-155, 1998.

Larraza, A., "An acoustic analog to the Einstein–Hopf drag," *unpublished,* 1999.

Longuet-Higgins, M. S., B. R. Kerman, and K. Lunde, "The release of air bubbles from an underwater nozzle," J. Fluid Mech. **230**, 365-390, 1991.

Rueda, A., "Model of Einstein and Hopf for protons in zero–point field and cosmic–ray spectrum," *Nuovo Cimiento* **48**, 155–183, 1978.

Rueda, A. and B. Haisch, "Inertia as reaction of the vacuum to accelerated motion," *Foundations of Physics* **28**, 1057-1108, 1998.

INITIAL DISTRIBUTION LIST

1. Defense Technical Information Center.....2
   8725 John J. Kingman Rd., STE 0944
   Ft. Belvoir, VA 22060-6218

2. Dudley Knox Library.....2
   Naval Postgraduate School
   411 Dyer Rd.
   Monterey, CA 93943-5101

3. Prof. A. Larraza, Code PH/La.....2
   Department of Physics
   Naval Postgraduate School
   Monterey, CA 93943-5002

4. Prof. B. Denardo, Code DH/Db.....2
   Department of Physics
   Naval Postgraduate School
   Monterey, CA 93943-5002

5. Prof. W. B. Colson, Code PH/Cw.....1
   Department of Physics
   Naval Postgraduate School
   Monterey, CA 93943-5002

6. Prof. J. Luscombe, Code PH/Lj.....1
   Department of Physics..
   Naval Postgraduate School
   Monterey, CA 93943-5002

7. Prof. W. Maier, Code PH/Mw.....1
   Department of Physics
   Naval Postgraduate School
   Monterey, CA 93943-5002

8. LT E. J. Chan 2
   Air Department
   USS Essex (LHD–2)
   FPO AP 96643–1661